جامعة الملك عبدالله
للعلوم والتقنية
King Abdullah University of
Science and Technology

# Correlating acceptor structure and blend nanostructure with the photostability of nonfullerene organic solar cells



| | |
|---|---|
| Item Type | Article |
| Authors | Paleti, Sri Harish Kumar;Hultmark, Sandra;Ramos, Nicolas;Gasparini, Nicola;Emwas, Abdul-Hamid M.;Martin, Jaime;Müller, Christian;Baran, Derya |
| Citation | Paleti, S. H. K., Hultmark, S., Ramos, N., Gasparini, N., Emwas, A.-H., Martin, J., Müller, C., & Baran, D. (2022). Correlating acceptor structure and blend nanostructure with the photostability of nonfullerene organic solar cells. Solar RRL. Portico. https://doi.org/10.1002/solr.202200436 |
| Eprint version | Post-print |
| DOI | 10.1002/solr.202200436 |
| Publisher | Wiley |
| Journal | Solar RRL |
| Rights | Archived with thanks to Solar RRL |
| Download date | 2025-05-12 15:52:54 |
| Link to Item | http://hdl.handle.net/10754/679893 |

Check for updates

# Correlating acceptor structure and blend nanostructure with the photostability of nonfullerene organic solar cells

Sri Harish Kumar Paleti[1], Sandra Hultmark[2], Nicolas Ramos[3], Nicola Gasparini[6], Abdul-Hamid Emwas[7], Jaime Martin[3,4,5], Christian Müller[2], and Derya Baran*[1]

[1] S. H. K. Paleti, Prof. D. Baran
King Abdullah University of Science and Technology (KAUST), Division of Physical Sciences and Engineering, and KAUST Solar Center (KSC), Thuwal 23955-6900, Saudi Arabia

[2] S. Hultmark, Prof. C. Müller
Department of Chemistry and Chemical Engineering, Chalmers University of Technology, Göteborg 41296, Sweden

[3] Nicolas Ramos, Dr. J. Martin
POLYMAT, University of the Basque Country UPV/EHU Av. de Tolosa 72, 20018, San Sebastián, Spain

[4] Prof. Jaime Martin
Ikerbasque Basque Foundation for Science Bilbao 481013, Spain

[5] Prof. Jaime Martin
Universidade da Coruña, Grupo de Polímeros, Departamento de Física e Ciencias da Terra, Centro de Investigacións Tecnolóxicas (CIT), Esteiro, 15471 Ferrol, Spain.

[6] Dr. N Gasparini
Department of Chemistry and Center for Plastic Electronics, Imperial College London, London W120BZ, UK

[7] Dr. A. H. Emwas
King Abdullah University of Science and Technology, Core Labs, Thuwal 23955, Saudi Arabia

Accepted Article

This article has been accepted for publication and undergone full peer review but has not been through the copyediting, typesetting, pagination and proofreading process, which may lead to differences between this version and the Version of Record. Please cite this article as doi: 10.1002/solr.202200436.

This article is protected by copyright. All rights reserved

Abstract

The formation of photo-induced traps resulting in the loss of electron mobility deteriorates the performance of organic solar cells under continuous light soaking. The genesis of these loss mechanisms is elucidated by examining the structural stability of halogenated ITIC derivative films and the phase behavior of the respective binary systems by blending with the donor polymer PBDBT-2F. Under constant illumination, ITIC-4Cl is found to maintain its structural integrity, whereas fluorine on the peripheral moieties of ITIC-4F undergo chemical substitution to form a mixture of ITIC and ITIC-4F. Thermal analysis of the light soaked binary films reveals that ITIC-4Cl loses its crystalline phase while the crystallinity of ITIC-4F does not undergo changes. Further, we show that the addition of a small amount of ITIC-4F as a third component hinders the loss of ITIC-4Cl crystalline phase in bulk-heterojunction blends through the formation of co-crystals. These results suggest that long-range ordering of NFAs does not necessarily improve the photo-stability of organic solar cells and that the addition of a third component, irrespective of the crystalline nature, can prevent changes in bulk-heterojunction blend nanostructure.

Accepted Article

Introduction:

Organic Solar Cells (OSC) offer a myriad of advantages including solution-processability and fabrication on flexible substrates,[1] enabling fast and cost-efficient manufacturing for opaque and

This article is protected by copyright. All rights reserved

semi-transparent architectures.[2] It unlocks a wide range of applications such as building-integrated photovoltaics, flexible integrated circuits for sensing applications,[3] agrivoltaics,[4] and solar windows.[5] State-of-the-art device efficiencies of lab-scale solution-processed OSCs have reached over 20%.[6] The improvement in device efficiencies is due to establishing design rules that permit to enhance photo-charge generation and minimize energy losses,[7] material innovation such as non-fullerene acceptors (NFA),[8] tuning of the active layer nanostructure,[9] and elegant device architectures such as tandem[10] and ternary solar cells.[11] Moreover, module efficiencies are faster than ever approaching the lab scale device efficiencies.[12] These advances create an urgency to improve the device lifetimes.

The formation of photo-induced traps under constant light soaking is the major reason for the deterioration of open-circuit voltages ($V_{oc}$) and fill factors ($FF$).[13] Both aging of the charge transport layers[14], photo-catalytic reactions induced by electron transport layers[15, 16] and the active layer[13] results in light induced trap formation. The aging of transport layers can be minimized by passivation[17] or by using UV-filters.[16] In case of fullerene based OSCs, the photo-induced trap formation in the bulk heterojunction (BHJ) is often assigned to fullerene dimerization,[13, 18] photolysis of the polymer under UV light exposure[19] and the amorphous nature of the donor polymer.[13] Studies dealing with the photo-aging of NFA based BHJ layers showed that the photo-stability and packing of NFAs[20] are critical parameters with regard to photostability. A recent study suggested that under constant light and at room temperature the short range ordered NFAs are prone to undergo diffusion limited crystallization and suffer from photo-induced trap formation.[20] However, the temperatures applied (room temperature) in these studies are much lower than the temperatures where diffusion limited crystallization starts to occur.[21]

Here, we explain the genesis of these photoinduced traps in ITIC-4F and ITIC-4Cl (see fig. 1 for chemical structures) based devices by carrying out a systematic investigation of the photostability of the respective acceptors and the phase behavior of blends BHJ. Nuclear magnetic resonance (NMR)

This article is protected by copyright. All rights reserved

Accepted Article

spectroscopy on the light soaked neat films of ITIC-4F and ITIC-4Cl suggests that ITIC-4Cl is photo-resilient and whereas ITIC-4F is unstable under constant exposure of white light. The fluorine of the peripheral groups undergoes photo-chemical substitution resulting in a mixture of ITIC and ITIC-4F. This suggests that ITIC-4F is inherently unstable to the constant exposure of light. Further, the nanostructure evaluation of fresh and photo-aged blend films of PM6, ITIC-4F and ITIC-4Cl (Chemical structures: fig. 1a) suggested a loss of crystalline order of ITIC-4Cl in PM6:ITIC-4Cl films, whereas ITIC-4F did not experience comparable changes. The addition of an amorphous third component, i.e. ITIC-4F to the PM6:ITIC-4Cl blend, hinders changes in the degree of crystalline order of ITIC-4Cl under constant illumination.

Results and discussion

We started the study by fabricating devices with an inverted architecture consisting of ITO/ZnO/active layer/$MoO_x$/Ag (fig. 1b) with an active layer thickness of approximately 100 nm. All active layers were spin-coated inside a glove box to minimize oxygen exposure. The PM6:ITIC-4F (1:1) device show a lower short-circuit current density ($J_{sc}$) than the PM6:ITIC-4Cl (1:1) device due to larger optical bandgap of ITIC-4F compared to ITIC-4Cl (fig. 1c). The B1 (open-circuit voltage, $V_{oc}$ = 0.84 V) based solar cells show a slightly higher $V_{oc}$ compared to the ITIC-4Cl counterpart ($V_{oc}$ = 0.79 V), despite a lower lowest unoccupied molecular orbital (LUMO) value of ITIC-4F (fig. 1d). The lower $V_{oc}$ of ITIC-4Cl based devices could be due to more energy losses or the energy mismatch of ITIC-4Cl LUMO levels with the work function of ETL layer.

Accepted Article

This article is protected by copyright. All rights reserved

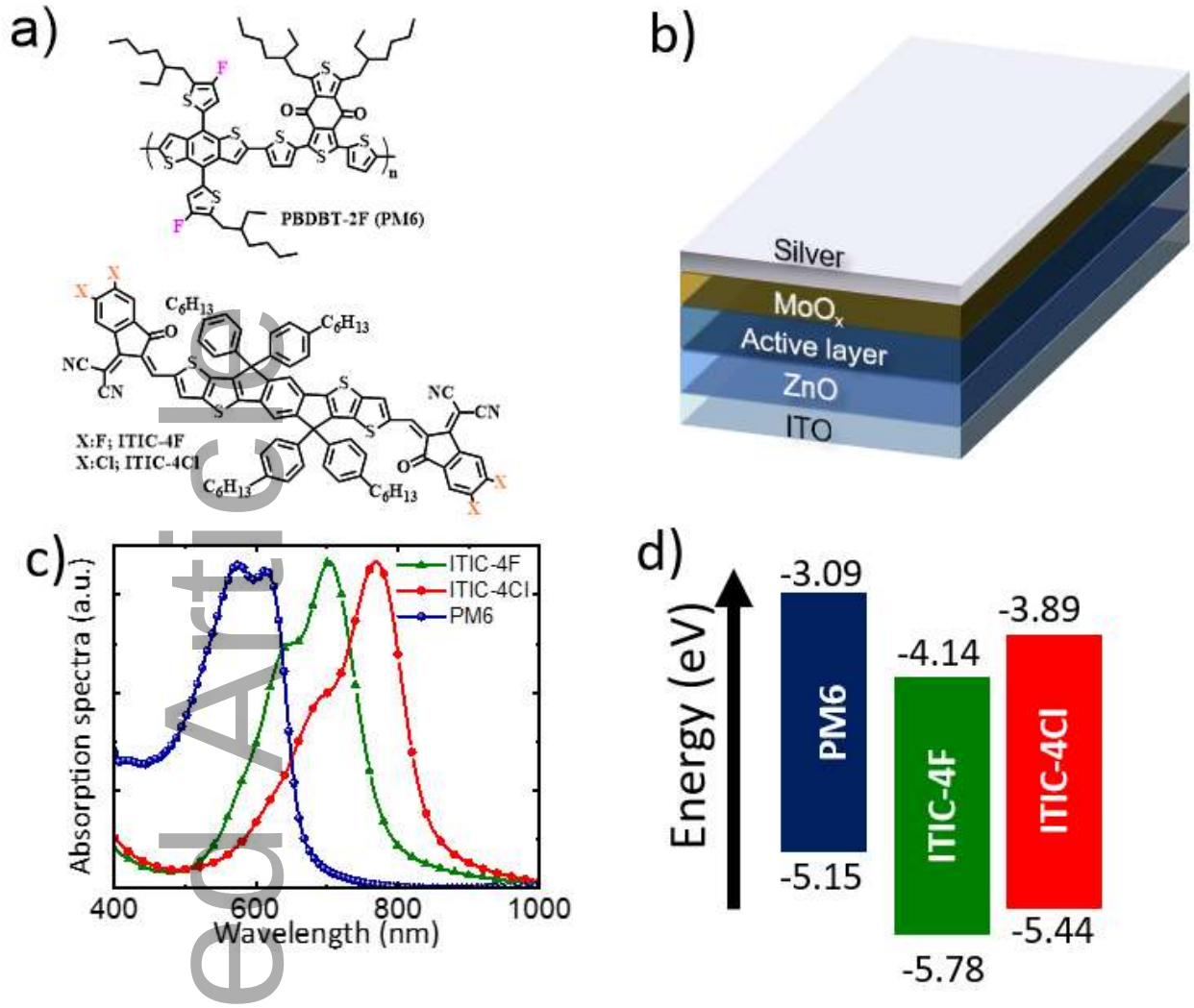


*Figure 1 a) Chemical structures of donor and acceptor molecules used in this study. b) Inverted device architecture employed in this study. c) Absorption spectra of the pristine films of PM6, ITIC-4F, and ITIC-4Cl. d) Ionization potential (IP) values measured on the pristine films by the photo-emission spectroscopy in the air (PESA). The electron affinities (EA) were calculated by subtracting optical bandgap from the IP respective IP values. The optical bandgap was measured using the absorption spectra of the respective materials.*

A slight improvement in the $J_{sc}$ of the ternary, PM6:ITIC-4F:ITIC-4Cl (1:0.2:0.8), in comparison to devices PM6:ITIC-4F (fig. 2a) is due to the better spectral response in the near infrared region (fig. 2b), which is due to broader absorption of the ternary blend in the 780 nm-810 nm (fig. S1). We note that the integrated $J_{sc}$ calculated from the EQE of these devices matches the measured $J_{sc}$ within a margin of 10%.

We carried out current-voltage measurements at different light intensities to elucidate the recombination dynamics of fresh devices (fig. 2 c-d). This technique provides information about the power-law dependence of $J_{sc}$ on the light intensity according to $J_{sc} \propto P_{in}^{S}$, where $S$ represents a power-law exponent and $P_{in}$ the light intensity. A linear dependence, i.e., $S = 1$, is indicative of 2nd

This article is protected by copyright. All rights reserved

Accepted Article

order recombination having a negligible effect on the extracted current, whereas S<1 suggests 2nd order recombination as a limiting factor. Whereas in the case of $V_{oc,}$ the light-dependence of $V_{oc}$ is related to the trap state formation.[22]

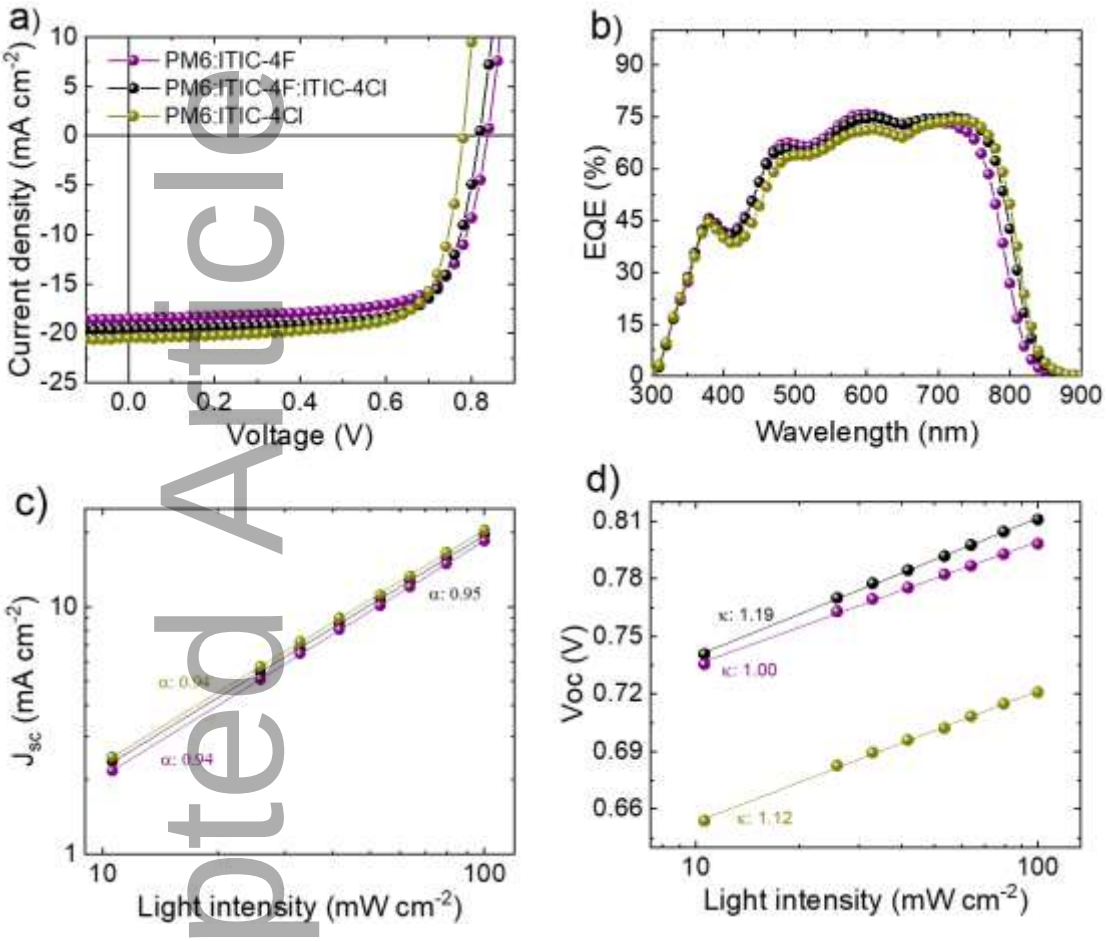


*Figure 2 a) Current density vs Voltage ($J-V$) curves of PM6:ITIC-4F, PM6:ITIC-4Cl and PM6:ITIC-4F:ITIC-4Cl based devices. The External quantum efficiency (EQE) curves of the respective solar cells. c) Short-circuit current density as a function of light intensity for fresh PM6:ITIC-4F, PM6:ITIC-4Cl and PM6:ITIC-4F:ITIC-4Cl devices. d) Open-circuit voltage as a function of light intensity for fresh binary and ternary devices.*

At room temperature, a slope of 1 $kT/q$ in a semi-logarithmic plot of $V_{oc}$ versus $P_{in}$ suggests a trap-free recombination, whereas, a slope of 2 $kT/q$ suggests a purely trap-assisted recombination.[31] The double-logarithmic $J_{sc}$ versus $P_{in}$ representative plot in fig. 2c, indicates that the slope is below unity and both binaries show a similar value ($\alpha$=0.95 for PM6:ITIC-4F:ITIC-4Cl and $\alpha$=0.94 for PM6:ITIC-4F and PM6:ITIC-4Cl). The values suggest that all three devices suffer from 2nd order recombination. In case of the $V_{oc}$ versus $P_{in}$ semi-logarithmic plot in fig. 2d, the PM6:ITIC-4F based solar cells feature a slope of 1 $kT/q$, which suggests that these devices do not feature trap-assisted

This article is protected by copyright. All rights reserved

Accepted Article

recombination, whereas the PM6:ITIC-4Cl and PM6:ITIC-4F:ITIC-4Cl devices give rise to a slope of 1.12 $kT/q$ and 1.19 $kT/q$ respectively, indicating almost pure 2nd order recombination.

*Table 1 Overview of photovoltaic device parameters of fresh devices*

| **Blends** | $J_{sc}$, **mA cm$^{-2}$** | $V_{oc}$, **V** | $FF$, **%** | $PCE$, **%** |
|---|---|---|---|---|
| PM6:ITIC-4F | 18.5±0.47 | 0.84±0.01 | 71.1±0.73 | 11.0±0.37 |
| PM6:ITIC-4F:ITIC-4Cl | 19.6±0.65 | 0.82±0.01 | 72.5±0.35 | 11.6±0.47 |
| PM6:ITIC-4Cl | 20.5±0.55 | 0.79±0.01 | 72.6±0.46 | 11.6±0.40 |

The binary and ternary devices were transferred to an environmental chamber to degrade the samples in controlled environment under MHI or LED lamps (see experimental section for more details) [23] at 1 sun condition. The evolution of the photovoltaic parameters under the respective lamps can be found in fig. 3 (a-d) and fig. S2 (a-d). Under MHI lamps the devices degraded much faster than under LED lamps, which could be due to crosslinking of the donor polymer triggered by the presence of UV-light in the MHI lamp spectrum.[19] Both PM6:ITIC-4F and PM6:ITIC-4Cl devices showed a considerable loss in the $FF$, whereas PM6:ITIC-4F:ITIC-4Cl devices were relatively less affected under constant illumination even after 710 h. All three light-soaked devices showed an increase in the slope of $V_{oc}$ Vs $P_{in}$ suggesting increased trap assisted recombination compared to the respective fresh devices (fig. S4). Among the three devices, PM6:ITIC-4F displayed a greater increase in slope, followed by PM6:ITIC-4Cl and finally the PM6:ITIC-4F:ITIC4Cl device. To evaluate the origin of the formation of photo-induced traps, chemical structure and nanostructure analysis of fresh and degraded films were performed.

Accepted Article

This article is protected by copyright. All rights reserved

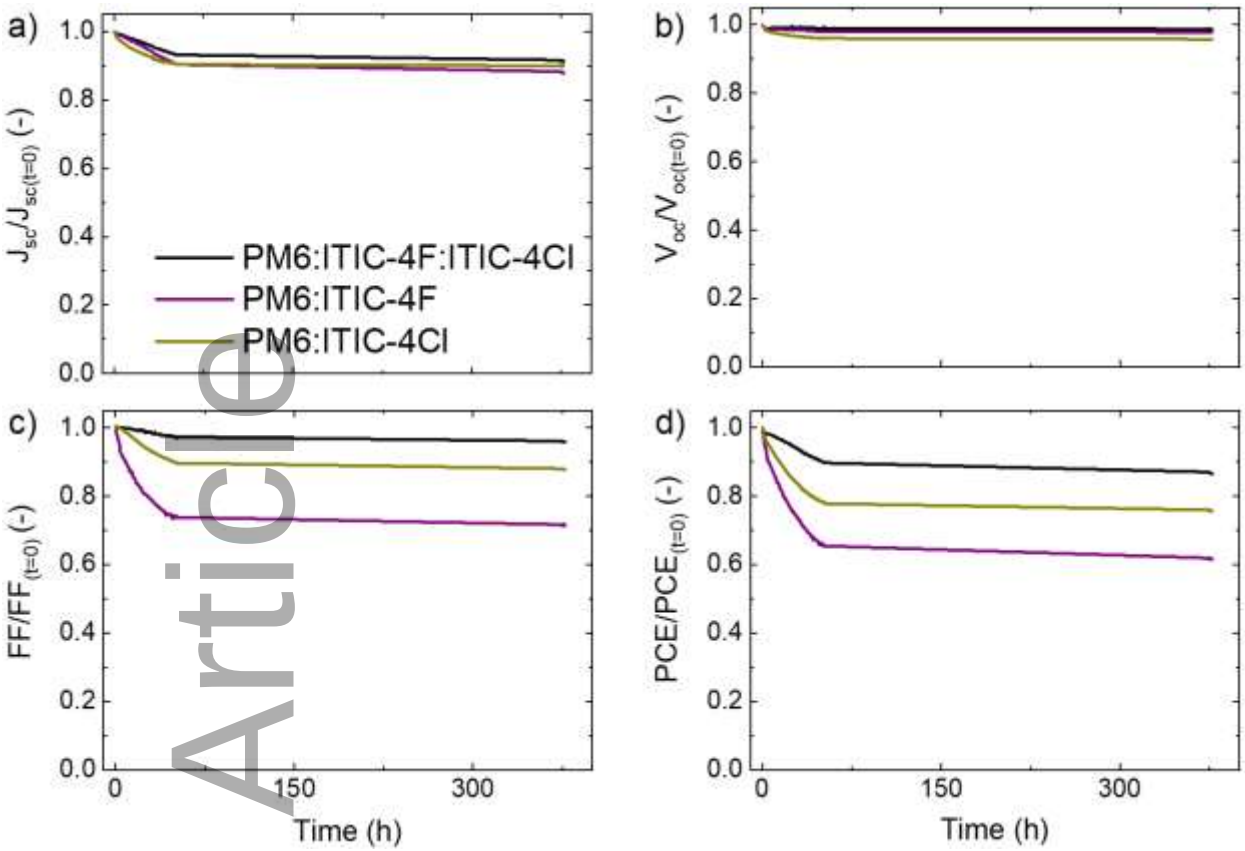


*Figure 3 Normalized parameters of $J_{sc}$ (a), $V_{oc}$ (b), FF (c), and PCE (d) of B1, B2, and T1 based solar cells for a duration of 710 h. The devices are illuminated by LED lights. The temperature of the devices during the light soaking is a maximum of 30 $^{o}$C (Fig.S4).*

We probed the light induced changes of ITIC-4F and ITIC-4Cl films by recording the absorption spectra at regular intervals (fig. 4a). The aging under constant light irradiation was conducted on silica glass slide in the absence of any additive. The ITIC-4F films displayed a loss in absorption whereas the spectra of ITIC-4Cl remained unchanged (fig. S5a). To confirm that, the changes are light induced, the absorption spectra of both acceptors stored in a dark and inert atmosphere. The optical density at the absorption maximum of ITIC-4F drops under constant illumination suggesting the changes in ITIC-4F are light induced (fig. S5b). To investigate the photo-induced chemical changes in more detail, nuclear Magnetic Resonance spectroscopy (NMR) (fig. 4b) and high-resolution mass spectroscopy (HR-MS) analysis were conducted on fresh and degraded ITIC-4F films. The assignment of the peaks observed in NMR spectra can be found in fig. S7 a-b. The comparison between fresh and degraded films suggests that the core group remains unchanged, i.e., IDTT. In contrast, the peripheral group of ITIC-4F changes from fluorine to hydrogen fig. 4b. These

This article is protected by copyright. All rights reserved

Accepted Article

differences suggest that under constant illumination, the fluorine atoms are replaced by hydrogen leading to the formation of ITIC as evident by the appearance of new peaks which are consistent with spectra recorded for neat ITIC (fig. 4b). The formation of ITIC is also confirmed by HR-MS (fig. S7 a-b). Instead, NMR confirmed that ITIC-4Cl films did not undergo any changes during light illumination (fig. S8).

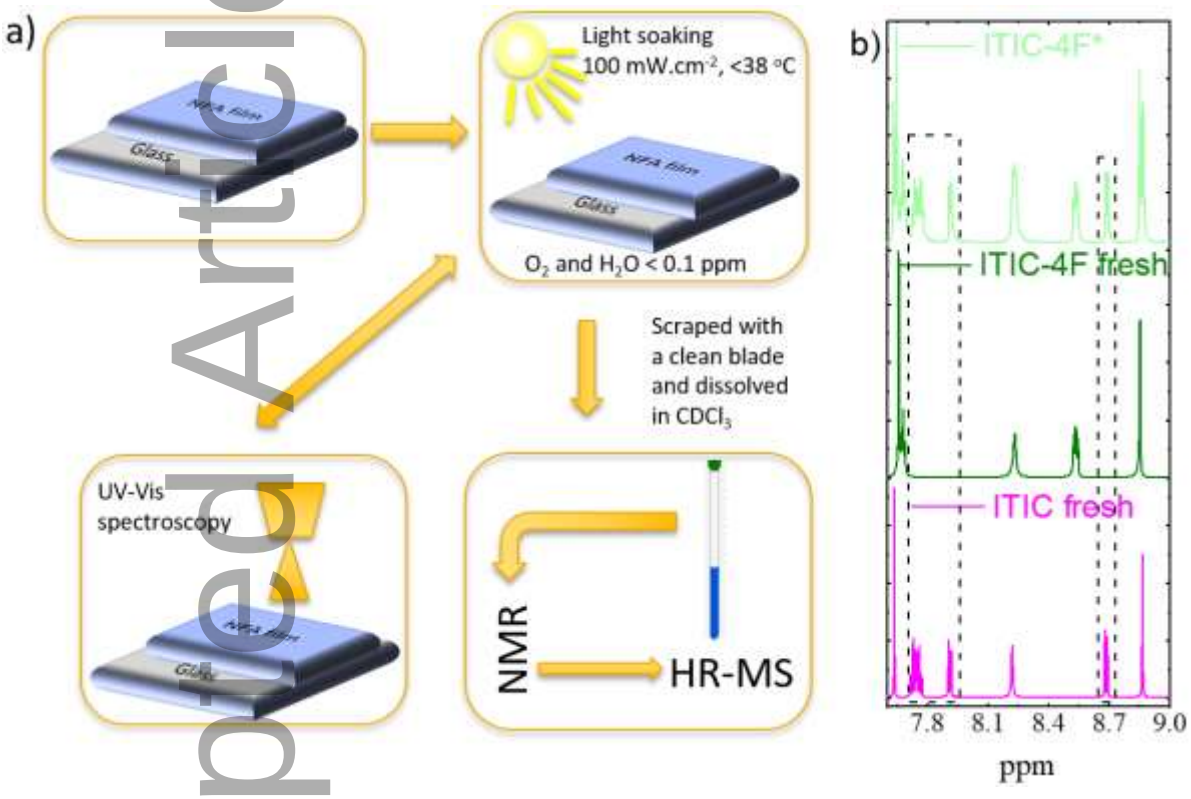


*Figure 4 a) Schematic representation of the general experimental methodology used to study the photodegradation of non-fullerene acceptors. (b) The NMR spectra of fresh and light-soaked ITIC-4F. ITIC-4F* represents the NMR peaks of light-soaked films. The NMR peaks of ITIC are assigned in Fig. S6c*

We analyzed the nanostructure by evaluating the phase behavior of the fresh acceptor and blend films using differential scanning calorimetry (DSC) and grazing incidence wide angle X-ray scattering (GIWAXS). ITIC-4Cl is more ordered than ITIC-4F reaching a higher degree of crystallinity during spin-coating at room temperature as explained in our previous work (fig. 5a and b)[24]. The two acceptors in PM6:ITIC-4F and PM6:ITIC-4Cl binary films undergo crystallization above their glass transition temperatures ($T_g$) as seen by the exothermic peaks at 200 ℃ and 220 ℃, respectively (fig. 5a; $T_g$ of ITIC-4F and ITIC-4Cl is 185℃ and 210℃, respectively).[24] The better packing of ITIC-4Cl

This article is protected by copyright. All rights reserved

Accepted Article

crystals explains the higher fill factors of PM6:ITIC-4Cl devices. The diffraction peaks observed for fresh PM6:ITIC-4F and fresh PM6:ITIC-4Cl blend in fig. 5b suggest that the degree of crystallinity of ITIC-4F and ITIC-4Cl is retained upon mixing with the donor polymer. Upon constant light soaking, no changes in the line-cuts of PM6:ITIC-4F (aged PM6:ITIC-4F, fig. 5b and S9) are observed, which suggests that the nanostructure of PM6:ITIC-4F films does not undergo any changes. In contrast, the disappearance of ITIC-4Cl diffraction peaks in line-cuts of aged PM6:ITIC-4Cl films suggests a loss of crystalline order in case of ITIC-4Cl. In addition, the crystallinity of the PM6 is also decreased under constant illumination. These changes in the nanostructure of the PM6:ITIC-4Cl blend are consistent with an increase in the number of photo-induced traps of PM6:ITIC-4Cl.

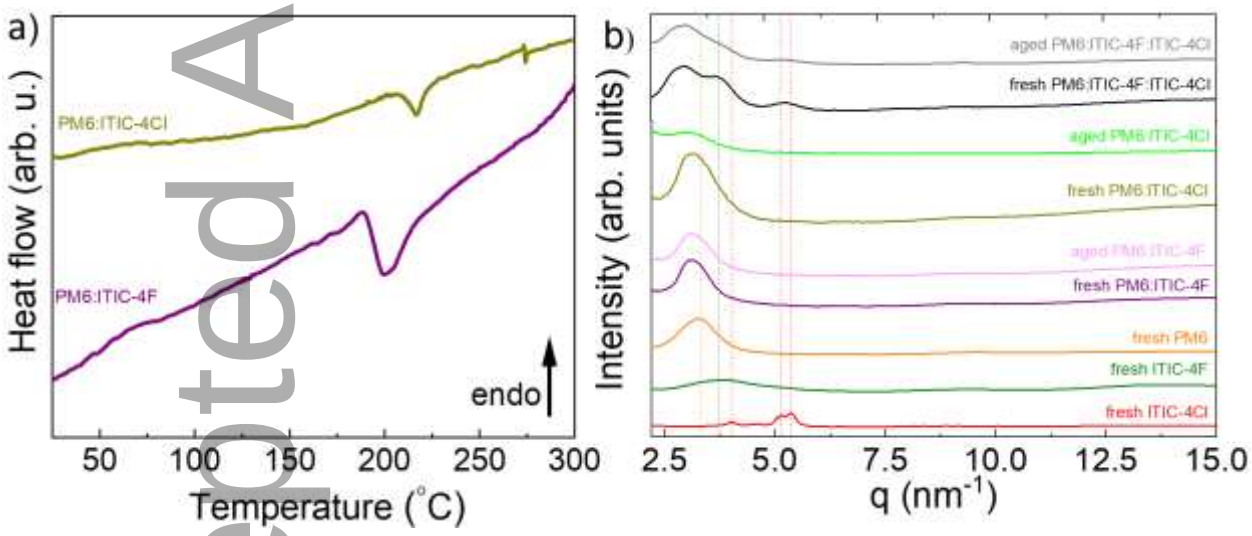


*Figure 5 a) DSC first heating thermograms of the PM6:ITIC-4F and PM6:ITIC-4Cl blends. b) line-cuts obtained by integration of GIWAXS patterns of different films. The line-cuts are normalized to the film thickness. The thickness of PM6:ITIC-4F (aged and fresh): 150 nm; PM6:ITIC-4Cl (aged and fresh): 84 nm; PM6:ITIC-4F:ITIC-4Cl (aged and fresh): 100 nm.*

We also explored the possibility to minimize the changes in the BHJ nanostructure through the addition of a third component, a strategy that is gaining attention because it allows to improve the operational stability of NFA based OSCs. GIWAXS diffractogram of ternary blend films indicate the presence of co-crystals of ITIC-4F and ITIC-4Cl[24]. We argue that the formation of acceptor co-crystals impedes the loss of crystalline material.

Accepted Article

This article is protected by copyright. All rights reserved

## Conclusion

In this study, we have shown that the poor photostability of ITIC-4F based OSC's is related to chemical changes of ITIC-4F and not related to changes in the nanostructure of B1 films under constant illumination. NMR spectroscopy and HR-MS analysis of 500 h photoaged films of ITIC-4F revealed the formation of a mixture of ITIC-4F and ITIC. Instead, ITIC-4Cl was found to be photo stable. The nanostructure of B2 was found to evolve upon constant illumination resulting in the formation of photo-induced traps. In case of PM6:ITIC-4Cl blend, both PM6 and ITIC-4Cl loses its crystalline order under constant illumination. This observation suggests that ordered NFA domains do not necessarily result in photo-stable devices. Moreover, we were able to show that the addition of ITIC-4F to ITIC-4Cl results in the formation of co-crystals, which results in a more photo-stable nanostructure.

## Experimental section

### Materials:

PBDBT-2F, PM6 (number-average molecular weight $\boldsymbol{M_n}$ ~ 19 kg mol$^{-1}$, polydispersity index PDI = 2.3), ITIC-4F and ITIC-4Cl were purchased from 1-materials Inc and used as received. Chlorobenzene was obtained from Sigma Aldrich and used as received. All samples are processed from a total concentration of 20 mg/ml chlorobenzene solutions. More details can be found in the respective sections.

### Differential scanning calorimetry (DSC):

Measurements were conducted with a DSC from Mettler Toledo equipped with a Gas controller GC 200 system at a heating rate of 10 $^{o}$C/min. Samples were prepared by drop-casting 4 mg of materials on a microscopy glass slide, followed by transfer to an Aluminum crucible.

### Grazing-incident wide-angle X-ray scattering (GIWAXS):

*Solution preparation:* PM6, ITIC-4F and ITIC-4Cl were stirred in chlorobenzene at 20 mg/ml overnight on a hot plate at 80 $^{o}$C in separate vials. The pristine solutions were blended in equal amounts to obtain respective blend solutions and stirred for 1 h at 80 $^{o}$C. After spin-coating the first set of films, the solution was left inside the glove box at room temperature. Then a small amount (10

This article is protected by copyright. All rights reserved

Accepted Article

$\mu l$) of chlorobenzene was added to maintain the same concentration and stirred at 80 °C on a hot plate.

*Film preparation for GIWAXS studies:* Two sets of films were fabricated by spin-coating the blend solutions on Si substrates. One set of films were spin-coated and left in an environment controlled degradation chamber. The conditions are mentioned below. The other set of samples were fabricated the day before shipping the films for GIWAXS characterization. Si substrates were cleaned by ultra-sonicating in IPA and acetone consecutively for 8 minutes each. Further cleaning in oxygen plasma for 5 minutes was done to remove any possible organic impurities. Later the blend films have deposited by spin-coating under nitrogen at 2000 rpm. The degradation was carried out as mentioned above.

*Experimental conditions:*

GIWAXS measurements were performed at the BL11 NCD-SWEET beamline at ALBA Synchrotron Radiation Facility (Spain). The incident X-ray beam energy was set to 12.4 eV using a channel-cut Si (1 1 1) monochromator. The angle of incidence $\alpha_i$ was set between 0.1-0.15° to ensure surface sensitivity. The scattering patterns were recorded using a Rayonix® LX255-HS area detector, which consists of a pixel array of 1920 × 5760 pixels (H × V) with a pixel size of 44 × 44 μm$^2$. Data are expressed as a function of the scattering vector ($q$), which was calibrated using $Cr_2O_3$ as a standard sample, obtaining a sample to detector distance of 219.56 mm. The exposure times of the samples were 5 s. 2D GIWAXS patterns were corrected as a function of the components of the scattering vector. Edges of the samples were removed to eliminate edge effects in the GIWAXS pattern.

*Optical characterization:* Absorption spectra of pristine films were measured using a Carry 5000 UV–vis–NIR spectrophotometer (Agilent Technologies).

*Nuclear Magnetic Resonance:*

Samples were prepared by dissolving the sample in 600 $\mu l$ of deuterated chloroform $CDCl_3$ inside a 3ml glass vial, the sample was vertex until the sample dissolves completely, then 500 $\mu l$ was

This article is protected by copyright. All rights reserved

Accepted Article

transferred to 5 mm NMR tube. All $^{13}C$ and $^{1}H$ NMR spectra were recorded using a Bruker 700 MHz AVANACIII NMR spectrometer equipped with Bruker CPTCI multinuclear *CryoProbe* (BrukerBioSpin, Rheinstetten, Germany). The $^{19}F$ NMR spectra were acquired using a Bruker 600 MHz AVANACIII NMR spectrometer equipped with a 5 mm Bruker BBOF probe (BrukerBioSpin, Rheinstetten, Germany). To create comparable data all $^{13}C$ NMR spectra were recorded using the zgig30 pulse program by collecting 24k scans with a recycle delay time of 10 s. The $^{1}H$ NMR spectra were recorded by collecting 64 scans with a recycle delay time of 10 s, using one pulse sequence through a standard (zg) program from the Bruker pulse library. Chemical shifts of both $^{1}H$ and $^{13}C$ were corrected using TMS signal at 0.0 pp, as internal chemical shift reference. All $^{19}F$ NMR spectra were measured under the same conditions and instrumental pampers using spin-echo with gradients sequence through a standard (zggpse) program. All spectra were recorded at room temperature and Bruker Topspin 3.5pl7 software was used to record the spectra and MestReNova software was used to analyze the data.

*Device fabrication:*

Pre-patterned Indium Tin Oxide (ITO) glass substrates were cleaned in an ultrasonic bath with acetone and isopropyl alcohol, dried under nitrogen flow, and treated with oxygen plasma for five minutes. 20 mg/ml of each of PM6, ITIC-4F, and ITIC-4Cl were dissolved in Chlorobenzene overnight at 80 ºC. The appropriate donor:acceptor(s) ratios (binary:1:1; ternary: 1:0.5:0.5) of each were stirred for a couple of hours before spin-coating the active layer. No additives were added to evade any possible additive-induced crystallization in the active layer. A ZnO sol-gel interlayer was deposited by spin coating, the recipe can be found elsewhere[34]. Active layers were spin-coated at 2000 rpm inside a glove box, followed by annealing as indicated. The thickness of the active layers is approximately 100 nm. Finally, 10 nm $MoO_x$ followed by 100 nm silver were thermally evaporated at $1*10^{-6}$ bar.

This article is protected by copyright. All rights reserved

Accepted Article

*Device characterization and light soaking tests:*
J–V curves were measured using Keithley 2400 source meter and a WaveLabs sinus-70 solar simulator calibrated to 1 sun, AM1.5 G. Light intensity measurements were carried using a neutral density filter purchased from Thor Labs. The intensity of light transmitted through the filter was independently measured via a Si reference cell. The photoaging test has been carried out in a homemade setup at 1 sun condition (AM 1.5G spectrum) in $N_2$. MHI lamps were used to simulate AM1.5G spectrum conditions.

Accepted Article

This article is protected by copyright. All rights reserved

Acknowledgments

S.H.K.P and D.B acknowledge the King Abdullah University of Science and Technology (KAUST) Office of Sponsored Research (OSR) under OSR-2018-CPF-4106 and OSR-2019-CARF/CCF-3079. S.H. and C.M. thank the Knut and Alice Wallenberg Foundation for funding through the project "Mastering Morphology for Solution-borne Electronics".

References

[1] G. D. Spyropoulos, P. Kubis, N. Li, D. Baran, L. Lucera, M. Salvador, T. Ameri, M. M. Voigt, F. C. Krebs, C. J. Brabec, Energy & Environmental Science 2014, 7, 3284.
[2] L. Lucera, F. Machui, P. Kubis, H. D. Schmidt, J. Adams, S. Strohm, T. Ahmad, K. Forberich, H. J. Egelhaaf, C. J. Brabec, Energy & Environmental Science 2016, 9, 89.
[3] E. Bihar, D. Corzo, T. C. Hidalgo, D. Rosas-Villalva, K. N. Salama, S. Inal, D. Baran, Advanced Materials Technologies 2020, 5, 2000226.
[4] E. Magadley, M. Teitel, M. F. Peretz, M. Kacira, I. Yehia, Sustainable Energy Technologies and Assessments 2020, 37, 100641.
[5] B. Lee, L. Lahann, Y. Li, S. R. Forrest, Sustainable Energy & Fuels 2020, 4, 5765.
[6] Z. Zheng, J. Wang, P. Bi, J. Ren, Y. Wang, Y. Yang, X. Liu, S. Zhang, J. Hou, Joule 2022, 6, 171.
[7] S. Karuthedath, J. Gorenflot, Y. Firdaus, N. Chaturvedi, C. S. P. De Castro, G. T. Harrison, J. I. Khan, A. Markina, A. H. Balawi, T. A. D. Peña, W. Liu, R.-Z. Liang, A. Sharma, S. H. K. Paleti, W. Zhang, Y. Lin, E. Alarousu, D. H. Anjum, P. M. Beaujuge, S. De Wolf, I. McCulloch, T. D. Anthopoulos, D. Baran, D. Andrienko, F. Laquai, Nature Materials 2021, 20, 378; A. Markina, K.-H. Lin, W. Liu, C. Poelking, Y. Firdaus, D. R. Villalva, J. I. Khan, S. H. K. Paleti, G. T. Harrison, J. Gorenflot, W. Zhang, S. De Wolf, I. McCulloch, T. D. Anthopoulos, D. Baran, F. Laquai, D. Andrienko, Advanced Energy Materials 2021, 11, 2102363; D. Baran, T. Kirchartz, S. Wheeler, S. Dimitrov, M. Abdelsamie, J. Gorman, R. S. Ashraf, S. Holliday, A. Wadsworth, N. Gasparini, P. Kaienburg, H. Yan, A. Amassian, C. J. Brabec, J. R. Durrant, I. McCulloch, Energy & Environmental Science 2016, 9, 3783.
[8] S. Holliday, R. S. Ashraf, A. Wadsworth, D. Baran, S. A. Yousaf, C. B. Nielsen, C.-H. Tan, S. D. Dimitrov, Z. Shang, N. Gasparini, M. Alamoudi, F. Laquai, C. J. Brabec, A. Salleo, J. R. Durrant, I. McCulloch, Nature Communications 2016, 7, 11585; J. Yuan, Y. Zhang, L. Zhou, G. Zhang, H.-L. Yip, T.-K. Lau, X. Lu, C. Zhu, H. Peng, P. A. Johnson, M. Leclerc, Y. Cao, J. Ulanski, Y. Li, Y. Zou, Joule 2019, 3, 1140.
[9] X. Jiao, L. Ye, H. Ade, Advanced Energy Materials 2017, 7, 1700084.
[10] J. Troughton, S. Neubert, N. Gasparini, D. R. Villalva, J. Bertrandie, A. Seitkhan, S. H. K. Paleti, A. Sharma, M. De Bastiani, E. Aydin, T. D. Anthopoulos, S. De Wolf, R. Schlatmann, D. Baran, Advanced Energy Materials 2021, 11, 2100166; L. Meng, Y. Zhang, X. Wan, C. Li, X. Zhang, Y. Wang, X. Ke, Z. Xiao, L. Ding, R. Xia, H.-L. Yip, Y. Cao, Y. Chen, Science 2018, 361, 1094.
[11] N. Gasparini, S. H. K. Paleti, J. Bertrandie, G. Cai, G. Zhang, A. Wadsworth, X. Lu, H.-L. Yip, I. McCulloch, D. Baran, ACS Energy Letters 2020, 5, 1371; X. Song, N. Gasparini, M. M. Nahid, S. H. K. Paleti, J.-L. Wang, H. Ade, D. Baran, Joule 2019, 3, 846.
[12] A. Distler, C. J. Brabec, H.-J. Egelhaaf, Progress in Photovoltaics: Research and Applications 2021, 29, 24.
[13] T. Heumueller, T. M. Burke, W. R. Mateker, I. T. Sachs-Quintana, K. Vandewal, C. J. Brabec, M. D. McGehee, Advanced Energy Materials 2015, 5, 1500111.
[14] C. H. Peters, I. T. Sachs-Quintana, J. P. Kastrop, S. Beaupré, M. Leclerc, M. D. McGehee, Advanced Energy Materials 2011, 1, 491.
[15] B. Liu, Y. Han, Z. Li, H. Gu, L. Yan, Y. Lin, Q. Luo, S. Yang, C.-Q. Ma, Solar RRL 2020, 5, 2000638.

This article is protected by copyright. All rights reserved

Accepted Article

[16] Y. Jiang, L. Sun, F. Jiang, C. Xie, L. Hu, X. Dong, F. Qin, T. Liu, L. Hu, X. Jiang, Y. Zhou, Materials Horizons 2019, 6, 1438.
[17] B. Liu, Y. Han, Z. Li, H. Gu, L. Yan, Y. Lin, Q. Luo, S. Yang, C.-Q. Ma, Solar RRL 2021, 5, 2000638.
[18] T. Heumueller, W. R. Mateker, A. Distler, U. F. Fritze, R. Cheacharoen, W. H. Nguyen, M. Biele, M. Salvador, M. von Delius, H.-J. Egelhaaf, M. D. McGehee, C. J. Brabec, Energy & Environmental Science 2016, 9, 247.
[19] O. R. Yamilova, I. V. Martynov, A. S. Brandvold, I. V. Klimovich, A. H. Balzer, A. V. Akkuratov, I. E. Kusnetsov, N. Stingelin, P. A. Troshin, Advanced Energy Materials 2020, 10, 1903163.
[20] X. Du, T. Heumueller, W. Gruber, O. Almora, A. Classen, J. Qu, F. He, T. Unruh, N. Li, C. J. Brabec, Advanced Materials 2020, 32, 1908305.
[21] L. Yu, D. Qian, S. Marina, F. A. A. Nugroho, A. Sharma, S. Hultmark, A. I. Hofmann, R. Kroon, J. Benduhn, D. M. Smilgies, K. Vandewal, M. R. Andersson, C. Langhammer, J. Martin, F. Gao, C. Muller, ACS Applied Material & Interfaces 2019, 11, 21766.
[22] X. Song, N. Gasparini, M. M. Nahid, S. H. K. Paleti, C. Li, W. Li, H. Ade, D. Baran, Advanced Functional Materials 2019, 29, 1902441; S. R. Cowan, A. Roy, A. J. Heeger, Physical Review B 2010, 82, 245207.
[23] N. Gasparini, M. Salvador, S. Strohm, T. Heumueller, I. Levchuk, A. Wadsworth, J. H. Bannock, J. C. de Mello, H.-J. Egelhaaf, D. Baran, I. McCulloch, C. J. Brabec, Advanced Energy Materials 2017, 7, 1700770.
[24] S. Hultmark, S. H. K. Paleti, A. Harillo, S. Marina, F. A. A. Nugroho, Y. Liu, L. K. E. Ericsson, R. Li, J. Martín, J. Bergqvist, C. Langhammer, F. Zhang, L. Yu, M. Campoy-Quiles, E. Moons, D. Baran, C. Müller, Advanced Functional Materials 2020, 30, 2005462.

**TOC**

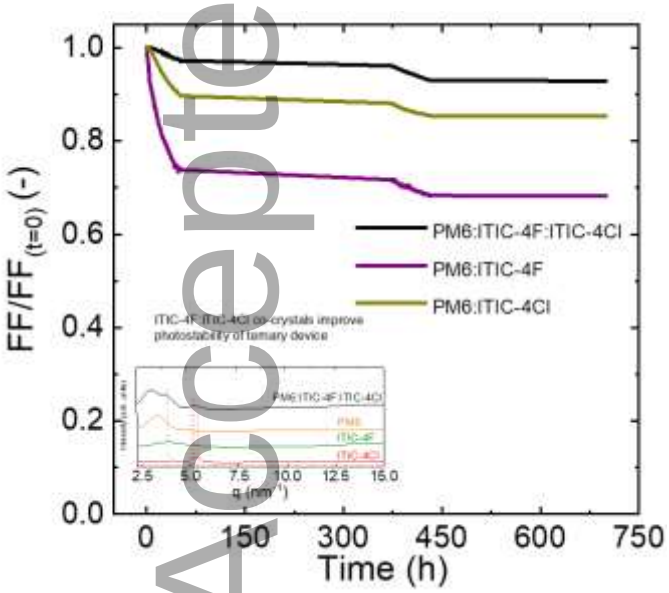


Here we show fill factor roll-off of binary and ternary solar cells with the best power conversion efficiency of 11.6%. By addition third component (ITIC-4F), we obtain an enhancement of photo-stability compared to the binary devices, PM6:ITIC-4F and PM6:ITIC-4Cl. This is because the addition of third component forms an acceptor co-crystal and inhibits the dissolution of ITIC-4Cl crystals.

Accepted Article

This article is protected by copyright. All rights reserved